



Comparative study of Rh–MoO_x and Rh–ReO_x supported on SiO₂ for the hydrogenolysis of ethers and polyols

Shuichi Koso^a, Hideo Watanabe^b, Kazu Okumura^c, Yoshinao Nakagawa^a, Keiichi Tomishige^{a,*}

^a School of Engineering, Tohoku University, 6-6-07 Aoba, Aramaki, Aoba-ku, Sendai, Miyagi 980-8579, Japan

^b Graduate School of Pure and Applied Sciences, University of Tsukuba, 1-1-1 Tennodai, Tsukuba, Ibaraki 305-8573, Japan

^c Department of Chemistry and Biotechnology, Graduate School of Engineering, Tottori University, Koyama-cho Minami, Tottori 680-8552, Japan

ARTICLE INFO

Article history:

Received 19 May 2011

Received in revised form 7 September 2011

Accepted 15 September 2011

Available online 21 September 2011

Keywords:

Metal–oxide interaction

Low valent Mo

Low valent Re

Hydrogenolysis

Regioselectivity

ABSTRACT

Rh–Mo_x/SiO₂ (M = Mo or Re) catalysts shows the high activity of the hydrogenolysis of C–O bond in the substrates with CH₂OH group such as tetrahydrofurfuryl alcohol, various diols and their ethers. Characterization results suggest the catalyst structure were isolated MoO_x species and small ReO_x cluster with low valence attached on the surface of Rh metal particles. It is characteristic that the reactivity of the C–O bond in the –O–C–CH₂OH is higher than that in the –O–C–CH₂OH over Rh–MoO_x/SiO₂, and Rh–ReO_x/SiO₂ has the opposite tendency to Rh–MoO_x/SiO₂. The difference in the regioselectivity of the hydrogenolysis over Rh–MoO_x/SiO₂ and Rh–ReO_x/SiO₂ can be related to the different structure of isolated MoO_x species and small ReO_x clusters.

© 2011 Elsevier B.V. All rights reserved.

1. Introduction

One effective method for the improvement in the catalytic performance of supported metal catalysts is the addition of another transition metal component to the catalysts. It is well known that the performance of metal catalyst may be much improved by the use of transition metal oxide supports such as TiO₂ [1,2]. The phenomenon are called strong metal support interaction (SMSI) and have been interpreted by the coverage of the surface of the metal particles with reduced support oxides, and the higher reducibility of the support oxide is connected to the stronger interaction. An important point is that partially reduced oxide species can strongly interact with noble metal surface. When reducible transition metal oxides are added to metal catalysts supported on irreducible oxide supports, the strong interaction between metal particles and reduced oxide species added has been observed, for example, in the case of silica-supported Rh–Mo, Rh–V, Rh–Nb systems, and this behavior is called as strong metal–oxide interaction [3–10].

The utilization of renewable resources as replacements of the fossil resources is essential for the sustainable development of our society. Because biomass is the only renewable source of organic carbon, biomass is a promising substitute for petroleum in the

production of fuels and plastics [11,12]. It is characteristic that biomass-derived chemicals often have high oxygen content and C–O bonds originated from hydroxide and ether groups. One of the strategies for the conversion of the biomass-derived chemicals is to strengthen the interaction between the OH group in the substrates and the catalyst surface via the oxide modifier on the surface of metal particles. We have recently found that Rh–ReO_x/SiO₂ catalysts are effective to the hydrogenolysis of tetrahydrofurfuryl alcohol (THFA) derived from hemi-cellulose [13]. The selectivity to 1,5-pentanediol is exceedingly by high (≈90%). The catalysts with only one component such as Rh/SiO₂ and ReO_x/SiO₂ are much less active and selective, indicating that the synergy between Rh and ReO_x brings about the high catalytic performance. The catalysts are also very active to the hydrogenolysis of glycerol which is a by-product of biodiesel from vegetable oils [14–16]. In contrast to the case of THFA, the selectivities are not high. The selectivities to 1,3-propanediol, 1,2-propanediol, 1-propanol and 2-propanol over Rh–ReO_x/SiO₂ (Re/Rh = 0.5) were 14, 42, 33 and 11%, respectively at 79% conversion. Characterization of Rh–ReO_x/SiO₂ with optimized Re/Rh ratio (0.5) by CO adsorption, TEM, TPR and EXAFS showed that the partially reduced ReO_x clusters are attached to the surface of Rh metal particles. Based on the kinetic analysis and product distribution in the hydrogenolysis of ethers, we have proposed the reaction mechanism where the hydride species formed at the interface between Rh metal surface and ReO_x cluster attacks the carbon atom neighboring the –CH₂OH group adsorbed on ReO_x clusters [17]. We have also reported that Rh–MoO_x/SiO₂

* Corresponding author. Tel.: +81 22 795 7214; fax: +81 22 795 7214.

E-mail address: tomi@erec.che.tohoku.ac.jp (K. Tomishige).

catalyzes the hydrogenolysis of THFA and glycerol [14–18]. In the THFA hydrogenolysis, the selectivity to 1,5-pentanediol is very high ($\leq 96\%$), like that over Rh–ReO_x/SiO₂. In the glycerol hydrogenolysis the selectivities to 1,3-propanediol, 1,2-propanediol, 1-propanol and 2-propanol over Rh–MoO_x/SiO₂ (Mo/Rh = 0.13) are 5, 37, 44 and 13%, respectively, at 39% conversion. Characterizations of Rh–MoO_x/SiO₂ with optimized Mo/Rh ratio (0.13) showed that partially reduced isolated Mo species are attached to the structure and the results of THFA hydrogenolysis suggests the similar reaction mechanism. However, the accurate comparison between Rh–ReO_x/SiO₂ and Rh–MoO_x/SiO₂ is difficult because detailed characterizations were only conducted for the catalysts with different Re/Rh and Mo/Rh ratio. In addition, low selectivities in the glycerol hydrogenolysis and their difference between Rh–ReO_x/SiO₂ and Rh–MoO_x/SiO₂ have not been fully explained.

This article is focusing on the accurate comparison between Rh–MoO_x/SiO₂ and Rh–ReO_x/SiO₂ with the same molar ratio of M (M = Mo or Re) to Rh, and the molar ratio of M/Rh = 0.13 was adopted. According to the catalyst characterization, Rh–MoO_x/SiO₂ (Mo/Rh = 0.13) and Rh–ReO_x/SiO₂ (Re/Rh = 0.13) gave similar Rh metal particle size and CO adsorption amount; on the other hand, different local structure around Mo or Re was detected by EXAFS catalysis. The comparison between these two catalysts in the catalytic performance in the hydrogenolysis of tetrahydrofurfuryl alcohol, various diols and their ethers enables the discussion on the effect of local structure of the oxide modifier on the catalytic performance in the hydrogenolysis reactions, which is contributable to the design of active sites for the selective conversion of biomass-derived alcohols and ethers.

2. Experimental

2.1. Catalyst preparation

A Rh/SiO₂ catalyst was prepared by impregnating SiO₂ with an aqueous solution of RhCl₃·3H₂O (Soekawa Chemical Co. Ltd.). The SiO₂ (G-6, BET surface area 535 m²/g) was supplied by Fuji Silysia Chemical Ltd. After the impregnation procedure and drying at 383 K for 12 h, they were calcined in air at 773 K for 3 h. Rh–Mo_x/SiO₂ (M = Re, Mo) catalysts were prepared by impregnating Rh/SiO₂ after the drying procedure with an aqueous solution of NH₄ReO₄ (Soekawa Chemical Co., Ltd.) or (NH₄)₆Mo₇O₂₄·4H₂O (Wako Pure Chemical Industries, Ltd.). ReO_x/SiO₂ and MoO_x/SiO₂ were also prepared by impregnation of SiO₂ with an aqueous solution of the same precursor as in the case of Rh–ReO_x/SiO₂ and Rh–MoO_x/SiO₂. These were calcined in air at 773 K for 3 h after drying at 383 K for 12 h. The loading amount of Rh was 4 wt.%, and that of additive was represented by the molar ratio of the additive to Rh. All catalysts were used in powdery form with granule size of <100 mesh.

2.2. Catalyst characterization

Temperature-programmed reduction (TPR) between 213 and 573 K was carried out in a fixed bed U-shaped reactor equipped with a thermal conductivity detector using 5% H₂ diluted with Ar (total 30 ml/min). The amount of catalyst was 0.01 g. The glass reactor loaded with the sample was cooled down to 177 K with frozen acetone. Next, H₂/Ar gas was introduced to the reactor. After removal of the frozen acetone bath, the reactor was quickly inserted in the electric furnace, and then the heating of the sample started at the rate of 5 K/min to 573 K.

The XRD patterns of the catalysts were recorded with Philips X'Pert MRD. The catalysts were filtrated after the activity, and dried overnight at room temperature, ground and put on the sample cell.

Average particle size of Rh metal was estimated using the Scherrer equation [19].

The amount of CO chemisorption was measured in a high-vacuum system using a volumetric method. Before adsorption measurements, the catalysts were treated in H₂ at 393 K for 1 h. Subsequently the adsorption was performed at room temperature. Gas pressure at adsorption equilibrium was about 1.1 kPa. The sample weight was about 0.1 g. The dead volume of the apparatus was about 60 cm³. Adsorption amount of CO is represented as the molar ratio to Rh and this value corresponds to the ratio of the surface Rh atoms to total Rh atoms assuming that the stoichiometry of adsorbed CO to surface Rh atom is one.

The extended X-ray absorption fine structure (EXAFS) spectra were measured at the BL01B1 station at SPring-8 with the approval of the Japan Synchrotron Radiation Research Institute (JASRI; proposal no. 2008B1235) and at the NW10A station at Photon Factory at the High Energy Accelerator Research Organization in Tsukuba, Japan (proposal no. 2007G070). The storage ring was operated at 8 and 6.5 GeV, respectively. A Si (1 1 1) single crystal and a Si (3 1 1) single crystal were used to obtain a monochromatic X-ray beam, respectively. Two ion chambers for I₀ and I were filled with Ar for Mo and Rh K-edge measurement. For Re L₃-edge measurement, I₀ and I ion chambers were filled with 85% N₂ + 15% Ar and 50% N₂ + 50% Ar, respectively. We measured the EXAFS spectra of the catalysts after the catalytic use. The catalytic reaction was carried out in an autoclave and under the following reaction conditions: 393 K reaction temperature, 8.0 MPa initial hydrogen pressure, 4 h reaction time, 20 ml of 5 wt.% tetrahydrofurfuryl alcohol (THFA) aqueous solution and 100 mg supported metal catalyst. The used catalyst powder and the solution were transferred together to the measurement cell without exposing air in the glove box. The thickness of the cell filled with the powder was 2 mm to give an edge jump of 0.1–0.4, 0.1–0.2 and 0.2–0.4 for Mo K-edge, Re L₃-edge and Rh K-edge measurement, respectively. The EXAFS data were collected in a transmission mode.

For EXAFS analysis, the oscillation was first extracted from the EXAFS data using a spline smoothing method [20]. Oscillation was normalized by the edge height around 50 eV. Fourier transformation of the *k*³-weighted EXAFS oscillation from the *k* space to the *r* space was performed to obtain a radial distribution function. The inversely Fourier filtered data were analyzed using a usual curve fitting method [21,22]. For curve fitting analysis, the empirical phase shift and amplitude functions for the Mo–O, Re–O, Re–Re and Rh–Rh bonds were extracted from data for Na₂MoO₄, NH₄ReO₄, Re powder and Rh foil, respectively. Theoretical functions for the Re–Rh, Rh–Re and Mo–Rh bonds were calculated using the FEFF8.2 program [23]. Analyses of EXAFS data were performed using a computer program (REX2000, ver. 2.5.9; Rigaku Corp.). Error bars for each parameter were estimated by stepping each parameter, while optimizing the others parameter, until the residual factor becomes two times as its minimum value [24].

2.3. Activity test of the hydrogenolysis reaction of ethers and polyols

Catalytic testing was performed in a 190 ml stainless steel autoclave with an inserted glass vessel. An aqueous solution of tetrahydrofurfuryl alcohol (THFA, Wako Pure Chemical Industries, Ltd.) was placed into the autoclaves with a spinner and an appropriate amount of catalysts. After sealing the reactors, their air content was purged by flushing thrice with 1 MPa hydrogen (99.99%; Takachiho Trading Co., Ltd.). Autoclaves were then heated to 393 K and pressurized to 1 MPa for the reduction pretreatment. The temperature was monitored using a thermocouple inserted in the autoclave. After 1 h, the H₂ pressure was increased to appropriate pressure at reaction temperature. During the experiment,

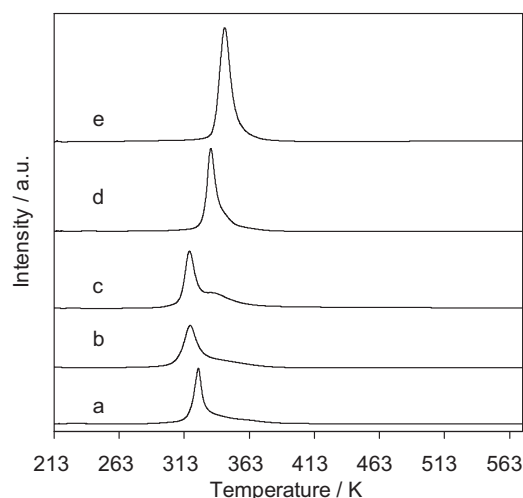


Fig. 1. TPR profile of Rh/SiO₂ (a), Rh–MoO_x/SiO₂ (Mo/Rh = 0.13 (b), 0.5 (c)), and Rh–ReO_x/SiO₂ (Re/Rh = 0.13 (d), 0.5 (e)).

the stirring rate was fixed at 500 rpm (magnetic stirring). It was checked that the change in the stirring rate did not affect the reaction when the rate was higher than 50 rpm. After an appropriate reaction time, the reactors were cooled down and all the gases were collected in a gas bag. The autoclave contents were transferred to vials, and the catalysts were separated by centrifugation and filtration. The standard conditions for the reaction were as follows: 393 K reaction temperature, 8.0 MPa initial hydrogen pressure, 2 or 4 h reaction time, 20 wt.% aqueous solution including 39 mmol THFA, and 50 mg supported metal catalyst. The products were analyzed using a gas chromatography (GC-17A; Shimadzu Corp.) equipped with FID. A Rtx[®]-1 PONA capillary column (diameter 0.25 mm ϕ , 100 m) was used for the separation. Products were also identified using GC–MS (QP5050, Shimadzu). The yields and selectivities were calculated on the carbon basis [17]. The hydrogenolysis of 2-ethoxyethanol, 2-butoxyethanol, 2-isopropoxyethanol, ethylene glycol, 1,2-propanediol, 1,2-butanediol, 2,3-butanediol, 1,3-propanediol, 1,3-butanediol, 2,4-pentanediol, 3-methoxy-1-propanol, 1,4-butanediol, 1,5-pentanediol and glycerol was also tested. All chemicals except for 2,4-pentanediol were supplied from Wako Pure Chemical Industries Ltd. and 2,4-pentanediol was purchased from Aldrich Chemical Co. Inc. The 20 wt.% aqueous solution containing 39 mmol substrate was applied to each activity test.

3. Results and discussion

3.1. Characterization of Rh–MoO_x/SiO₂ with different M/Rh ratio (M: Re, Mo)

3.1.1. TPR profile

Fig. 1 shows the TPR profiles of Rh/SiO₂, Rh–MoO_x/SiO₂ and Rh–ReO_x/SiO₂ catalysts calcined at 773 K. The amount of H₂ consumption is listed in Table 1. Rh–MoO_x/SiO₂ is reduced more easily than Rh/SiO₂ and Rh–ReO_x/SiO₂. Therefore, the starting temperature was set at 213 K to avoid the reduction before heating. The results of Rh/SiO₂ and Rh–ReO_x/SiO₂ (Re/Rh = 0.5) are essentially the same as those of the cases where the heating started at room temperature [14]. The amount of H₂ consumption of Rh/SiO₂ agreed with the stoichiometry of the reduction of Rh₂O₃. The amount of H₂ consumption of Rh–ReO_x/SiO₂ (Re/Rh = 0.5) corresponded to the partial reduction of ReO_x to the valence of around 3 in addition to the total reduction of Rh₂O₃. The profile had no peak in the temperature range where the reduction of ReO_x/SiO₂ [25–27] proceeded (533–553 K). The profile of Rh–ReO_x/SiO₂ (Re/Rh = 0.13) also

contained only one peak below the temperature range of ReO_x/SiO₂ reduction. The amount of H₂ consumption corresponded to the formation of partially-oxidized ReO_x species with the valence of 2–3. The profiles of Rh–MoO_x/SiO₂ (Mo/Rh = 0.13, 0.5) contained peaks below the temperature range of MoO_x/SiO₂ reduction (708–713 K) [28,29]. The amount of H₂ consumption corresponded to the formations of MoO_x species with Mo valence of around 4 from MoO₃ and Rh metal from Rh₂O₃ for both Rh–MoO_x/SiO₂ catalysts. These data suggested that all the added Mo and Re species in the catalyst with different amount of Mo or Re was affected by the presence of Rh species and the reduction of Mo and Re species was promoted probably via spilt-over hydrogen species from Rh to Mo and Re [30,31]. It should be noted that the reduction was completed at about 393 K for all the Rh-containing catalysts under 5% H₂. This shows that the pretreatment conditions (1 MPa H₂, 393 K, 1 h) were sufficient for the reduction of the catalysts as much as possible.

3.1.2. Particle size of Rh metal over Rh/SiO₂, Rh–MoO_x/SiO₂ and Rh–ReO_x/SiO₂

TPR profiles indicate that Rh species is reduced to the metallic state. In the XRD patterns of Rh/SiO₂, Rh–MoO_x/SiO₂ and Rh–ReO_x/SiO₂ after the catalytic use in the THFA hydrogenolysis, the peak around $2\theta = 41^\circ$ assigned to Rh metal was detected (Fig. S1, supporting information). Table 2 lists the average size of Rh metal phase on the catalysts, and it is concluded that Rh metal particle size is not influenced by the presence of MoO_x and ReO_x. Another important point is that the peak due to Mo and Re species was not detected. This indicates that the Mo and Re species is highly dispersed. Similar behavior has been observed on the Ir–ReO_x/SiO₂ catalysts [26,27].

3.1.3. The amount of CO adsorption

We had already reported that the CO adsorption amount (CO/Rh is decreased) by the addition of MoO_x and ReO_x, which is explained by the partial coverage of the surface of Rh metal particles with Mo or Re species (Table 2) [13,14,18,25,32]. In this article, we performed the detailed comparison between the dispersion which was estimated by XRD (Rh_s/Rh; molar ratio of the surface Rh atoms to total Rh atoms) and the results of CO adsorption (CO/Rh). Here, we have to pay attention to the difference between Rh_s/Rh and CO/Rh. The difference (Rh_s/Rh) – (CO/Rh) is interpreted by the coverage ratio of Rh surface with MoO_x and ReO_x. In the range of Mo/Rh and Re/Rh \leq 0.13, (Rh_s/Rh) – (CO/Rh) almost agrees with the molar ratio of Mo/Rh and Re/Rh, and this agreement means that all the added Mo and Re suppress the CO adsorption. The stoichiometry of the suppression of CO adsorption by the MoO_x and ReO_x covering is one Mo or Re atom to one CO adsorption site of Rh. At the same time, this means that all added Mo and Re atoms interacted with Rh metal surface and this also means the absence of Mo and Re species supported on the SiO₂ surface without the interaction with the Rh metal surface. On the other hand, in the range of Mo/Rh and Re/Rh $>$ 0.13, (Rh_s/Rh) – (CO/Rh) is smaller than the molar ratio of Mo/Rh and Re/Rh, suggesting that a part of added Mo and Re did not contribute to the suppression of CO adsorption by the way such as the formation of multilayer structure and the location on the support. Therefore, the comparison between Rh–MoO_x/SiO₂ and Rh–ReO_x/SiO₂ should be performed in the range of Mo/Rh and Re/Rh \leq 0.13.

3.1.4. EXAFS analysis

In order to characterize the interaction of Mo or Re species with Rh metal particles, Mo K-edge, Re L₃-edge, and Rh K-edge EXAFS analyses were carried out. Fig. 2 shows the Mo K-edge EXAFS analysis of Rh–MoO_x/SiO₂ catalysts after the catalytic use in the THFA hydrogenolysis, and the curve fitting results are shown in Table 3. Here, in the EXAFS analysis, it is theoretically impossible to

Table 1
Results of TPR profiles of the catalysts.

Catalyst	Mo/Rh or Re/Rh molar ratio	Loading amount (mmol g-cat ⁻¹)			H ₂ consumption ^a (mmol g-cat ⁻¹)	Valence of Mo or Re ^b
		Rh	Mo	Re		
Rh/SiO ₂	–	0.39	–	–	0.56	–
Rh–MoO _x /SiO ₂	0.13	0.39	0.05	–	0.64	3.7
	0.5	0.39	0.20	–	0.78	3.9
Rh–ReO _x /SiO ₂	0.13	0.39	–	0.05	0.70	2.4
	0.5	0.39	–	0.20	0.97	2.9

^a H₂ consumption in the range of 213–393 K.
^b Initial valence of Mo and Re before TPR is +6 and +7, respectively. Valence of Mo and Re after the reduction at 393 K is calculated by initial valence $-2 \times (\text{H}_2 \text{ consumption [mol]} - (\text{Rh amount [mol]} \times 3/2)/(\text{Mo or Re amount [mol]}))$.

Table 2
Results of XRD and CO adsorption of the reduced catalysts.

Catalyst	Mo/Rh or Re/Rh	Particle size XRD (nm)	Dispersion ^a XRD [Rh _s /Rh]	CO adsorption CO/Rh	Rh _s /Rh–CO/Rh
Rh/SiO ₂	–	2.8	0.39	0.39 ^{b,c}	0.0
Rh–MoO _x /SiO ₂	0.06	2.7	0.41	0.34 ^b	0.07
	0.13	2.6	0.42	0.29 ^{b,d}	0.13
	0.25	2.5	0.44	0.25 ^b	0.19
	0.5	2.7	0.41	0.18	0.23
Rh–ReO _x /SiO ₂	0.13	2.7	0.41	0.28 ^b	0.13
	0.25	2.7	0.41	0.23 ^b	0.18
	0.5	3.2	0.34	0.17 ^{b,c}	0.17

^a Rh_s/Rh = 1.098 nm/particle size [38].
^b Ref. [15].
^c Ref. [13].
^d Ref. [14].

Table 3
Curve fitting results of Mo K-edge EXAFS of various Rh–MoO_x/SiO₂ after the catalytic use.

Mo/Rh	Shells	CN ^a	<i>R</i> (×10 ⁻¹ nm) ^b	<i>σ</i> (×10 ⁻¹ nm) ^c	Δ <i>E</i> ₀ (eV) ^d	<i>R</i> _f (%) ^e
0.06	Mo–O	0.9 ± 0.5	2.01 ± 0.09	0.065 ± 0.050	–10.4 ± 15.4	0.8
	Mo–Rh(or –Mo)	3.5 ± 1.0	2.65 ± 0.02	0.080 ± 0.008	–3.5 ± 2.0	
0.13	Mo–O	1.1 ± 0.8	2.08 ± 0.05	0.061 ± 0.040	–2.8 ± 12.0	0.8
	Mo–Rh(or –Mo)	3.0 ± 1.1	2.64 ± 0.02	0.089 ± 0.020	–5.9 ± 3.0	
0.25	Mo–O	1.7 ± 0.5	2.03 ± 0.02	0.084 ± 0.017	–10.5 ± 2.4	0.3
	Mo–Rh(or –Mo)	2.3 ± 0.3	2.64 ± 0.01	0.094 ± 0.004	–6.0 ± 1.3	
0.5	Mo–O	2.6 ± 0.6	2.04 ± 0.04	0.090 ± 0.015	–10.5 ± 5.2	1.2
	Mo–Rh(or –Mo)	1.4 ± 0.4	2.62 ± 0.02	0.100 ± 0.012	–8.1 ± 3.9	

^a Coordination number.
^b Bond distance.
^c Debye–Waller factor.
^d Difference in the origin of photoelectron energy between the reference and the sample.
^e Residual factor. Fourier filtering range: 0.129–0.276 nm.

distinguish between Mo and Rh as a backscattering atom because the atomic number of Rh and Mo is similar [33]. Based on the presence of Mo–Rh interaction from the above characterization results, the amplitude and phase shift function of Mo–Rh calculated by FEFF was applied, and the results are represented by Mo–Rh (or –Mo). The presence of Mo–O and Mo–Rh (or –Mo) bonds was detected, and the bond distance of Mo–O is assigned to the single Mo–O bond, and an interesting point is that the bond distance of Mo–Rh (or –Mo) bond (0.262–0.265 nm) is comparable to that of Mo–Mo bond in Mo metal (0.267 nm) and Rh–Rh bond in Rh metal (0.268 nm). This represents that the Mo atoms directly interacted with Rh or other Mo atoms, unlike the Mo–O–Rh or Mo–O–Mo, although the Mo–O bond is detected. The coordination number (CN) of the Mo–O and the Mo–Rh (or –Mo) bonds was almost constant in the range of Mo/Rh ≤ 0.13. In contrast, the CN of the Mo–O bond increased and that of Mo–Rh (or –Mo) bond decreased with increasing Mo/Rh in the range of Mo/Rh > 0.13. This suggests that a part of the added

Mo species is present on the SiO₂ support and it is not interacted with Rh metal surface. This behavior is related to the deviation of (Rh_s/Rh) – (CO/Rh) from Mo/Rh in the range of Mo/Rh ≥ 0.25 in Table 2.

Fig. 3 shows the Re L₃-edge EXAFS spectra of Rh–ReO_x/SiO₂ after the catalytic use in the THFA hydrogenolysis. Table 4 summarizes the curve fitting results. The curve fitting results indicates that the presence of the Re–O, Re–Rh and Re–Re bonds. Unlike the case of Rh–MoO_x/SiO₂, it is easy to distinguish between Rh and Re as a scattering atom. We tried to fit the spectra using two different bonds (Re–O + Re–Rh and Re–O + Re–Re), however, we cannot get a good fit. Therefore, we fitted the spectra with three different bonds (Re–O + Re–Rh + Re–Re) (Fig. S2 and Table S1, supporting information). The presence of the Re–O bond indicates that Re species is in the partially oxidized state, which is supported by the TPR results above and Re L₃-edge XANES analysis reported in our previous reports [14]. The length of Re–O bond (0.210–0.213 nm)

Table 4Curve fitting results of Re L₃-edge EXAFS of various Rh–ReO_x/SiO₂ after the catalytic use.

Re/Rh	Shells	CN ^a	<i>R</i> (×10 ^{−1} nm) ^b	<i>σ</i> (×10 ^{−1} nm) ^c	Δ <i>E</i> ₀ (eV) ^d	<i>R</i> _f (%) ^e
0.13	Re–O	0.6 ± 0.4	2.13 ± 0.06	0.060 ± 0.050	10.0 ± 15.0	1.8
	Re–Rh	3.8 ± 2.7	2.66 ± 0.02	0.060 ± 0.020	9.7 ± 4.3	
	Re–Re	2.0 ± 1.4	2.71 ± 0.08	0.060 ± 0.050	−0.7 ± 15.0	
0.25	Re–O	1.2 ± 0.4	2.10 ± 0.02	0.061 ± 0.030	9.7 ± 5.0	0.3
	Re–Rh	3.6 ± 0.8	2.67 ± 0.01	0.063 ± 0.008	9.9 ± 2.0	
	Re–Re	2.2 ± 1.8	2.73 ± 0.04	0.060 ± 0.025	8.5 ± 5.0	
0.5	Re–O	1.3 ± 0.9	2.13 ± 0.11	0.099 ± 0.070	10.8 ± 8.8	1.0
	Re–Rh	3.6 ± 0.8	2.68 ± 0.01	0.063 ± 0.014	10.9 ± 1.9	
	Re–Re	2.8 ± 2.0	2.73 ± 0.03	0.064 ± 0.040	2.6 ± 5.3	

^a Coordination number.^b Bond distance.^c Debye–Waller factor.^d Difference in the origin of photoelectron energy between the reference and the sample.^e Residual factor. Fourier filtering range: 0.129–0.301 nm.**Table 5**Curve fitting results of Rh K-edge EXAFS of various Rh–MoO_x/SiO₂ and Rh–ReO_x/SiO₂ after the catalytic use.

Catalyst	Mo/Rh or Re/Rh	Shells	CN ^a	<i>R</i> (10 ^{−1} nm) ^b	<i>σ</i> (10 ^{−1} nm) ^c	Δ <i>E</i> ₀ (eV) ^d	<i>R</i> _f (%) ^e
Rh/SiO ₂	–	Rh–Rh	9.8 ± 1.5	2.67 ± 0.01	0.071 ± 0.004	−0.2 ± 1.7	0.3
Rh–MoO _x /SiO ₂	0.06	Rh–Rh (or –Mo)	10.1 ± 0.7	2.68 ± 0.01	0.075 ± 0.002	−0.9 ± 1.7	0.2
	0.13	Rh–Rh (or –Mo)	10.6 ± 0.8	2.68 ± 0.01	0.077 ± 0.002	0.2 ± 1.7	0.2
	0.25	Rh–Rh (or –Mo)	10.7 ± 1.0	2.68 ± 0.01	0.080 ± 0.003	−0.3 ± 2.2	0.4
	0.5	Rh–Rh (or –Mo)	10.5 ± 0.9	2.67 ± 0.01	0.083 ± 0.002	0.7 ± 1.8	0.3
Rh–ReO _x /SiO ₂	0.13	Rh–Rh	9.0 ± 0.7	2.68 ± 0.01	0.070 ± 0.003	0.6 ± 1.0	0.1
		Rh–Re	0.6 ± 0.5	2.66 ± 0.04	0.071 ± 0.030	−10.1 ± 15.0	
	0.25	Rh–Rh	9.4 ± 0.6	2.68 ± 0.01	0.074 ± 0.002	1.6 ± 0.6	0.1
		Rh–Re	1.0 ± 0.5	2.67 ± 0.03	0.080 ± 0.015	−6.4 ± 6.0	
	0.5	Rh–Rh	9.0 ± 0.9	2.68 ± 0.01	0.072 ± 0.003	−2.2 ± 1.2	0.1
		Rh–Re	1.7 ± 0.8	2.67 ± 0.04	0.092 ± 0.032	−10.0 ± 18.0	

^a Coordination number.^b Bond distance.^c Debye–Waller factor.^d Difference in the origin of photoelectron energy between the reference and the sample.^e Residual factor. Fourier filtering range: 0.166–0.291 nm (Rh/SiO₂, Rh–MoO_x/SiO₂), 0.153–0.288 nm (Rh–ReO_x/SiO₂).

on Rh–ReO_x/SiO₂ was longer than that (0.174 nm) on NH₄ReO₄, and the longer Re–O bond can be assigned to a single bond. The presence of Re–Rh bond demonstrates the interaction between Re species and Rh metal particles, and the bond length of the Re–Rh bond (0.266–0.268 nm) was similar to that of Rh–Rh bond (0.268 nm) in Rh foil and it was shorter than that of Rh–(O)–Rh bond (0.301 nm) in Rh₂O₃ [34,35]. This comparison indicates that the short Re–Rh bond is explained by the direct interaction like the case of Rh–MoO_x/SiO₂. Another important point is the presence of Re–Re bond. The bond length of the Re–Re bond (0.271–0.273 nm) on Rh–ReO_x/SiO₂ was comparable to that of the Re–Re bond (0.274 nm) in the Re metal and this indicates that no oxygen atoms are located between Re atoms. The coordination number (CN) (3.3–3.8) of the Re–Rh bond can be explained by the adsorption of Re atoms at three-fold hollow site of (111) surface and/or at four-fold hollow site of (100) surface. On the other hand, the CN of the Re–Re bond increased gradually with increasing the amount of Re. The CN (2.0–2.8) of the Re–Re bond is due to clustering of adsorbed Re species on the surface of Rh metal particles, at the same time, it is suggested that the size of the ReO_x clusters increases with increasing the additive amount of Re. Furthermore, the almost constant CN of the Re–Rh bond in the range of Re/Rh ≤ 0.5 suggests that the ReO_x clusters have 2-dimensional structure on the Rh metal surface. In the case of Rh–ReO_x/SiO₂, the CN of Re–Rh bond did not decrease with increasing Re/Rh so significantly, compared to the CN of Mo–Rh (or –Mo) on Rh–MoO_x/SiO₂. This tendency suggests that a part of Re species located on Rh metal surface without the suppression of CO adsorption is present. At present, we think that a part of Re species can

be located at the interface between Rh metal particles and SiO₂ support.

Another important point is that the CN (3.0) of Mo–Rh (or –Mo) on Rh–MoO_x/SiO₂ (Mo/Rh = 0.13) was much smaller than the CN (5.8 = 3.8 + 2.0) of Re–Rh + Re–Re on Rh–ReO_x/SiO₂ (Re/Rh = 0.13), although both Rh metal particle size and the amount of CO adsorption were almost the same on both catalysts. The different CN shows the different local structure around Mo and Re atoms. The small CN of the Mo–Rh (or –Mo) can be interpreted by the isolated Mo species on Rh metal surface, for example, three-fold hollow site of Rh (111) surface.

The reason for the different structure of Rh–MoO_x/SiO₂ (Mo/Rh = 0.13) and Rh–ReO_x/SiO₂ (Re/Rh = 0.13) is not elucidated and further investigation is necessary. At present, we think that the different structure is due to the different valence of Mo and Re. The valence of Mo is higher than that of Re, and the stronger repulsion by higher valence makes the Mo species isolated considering from the valence of Mo and Re (Table 1).

Fig. 4 shows the Rh K-edge EXAFS spectra of Rh/SiO₂ and Rh–MoO_x/SiO₂ (M = Mo or Re) after the catalytic use in the THFA hydrogenolysis. Table 5 summarizes the curve fitting results. The CN (9.8) of the Rh–Rh bond in Rh/SiO₂ is very smaller than that of bulk of Rh metal with fcc structure (CN = 12). This indicates that the Rh metal particle on SiO₂ is very small, and this result is supported by the results of XRD and CO adsorption amount. The CN (10.1–10.7) of the Rh–Rh (or –Mo) in various Rh–MoO_x/SiO₂ catalysts is nearly equal to that of Rh/SiO₂, however, the Debye–Waller factor of Rh–MoO_x/SiO₂ increased as the added amount of Mo increased. This is explained by the high static disorder probably

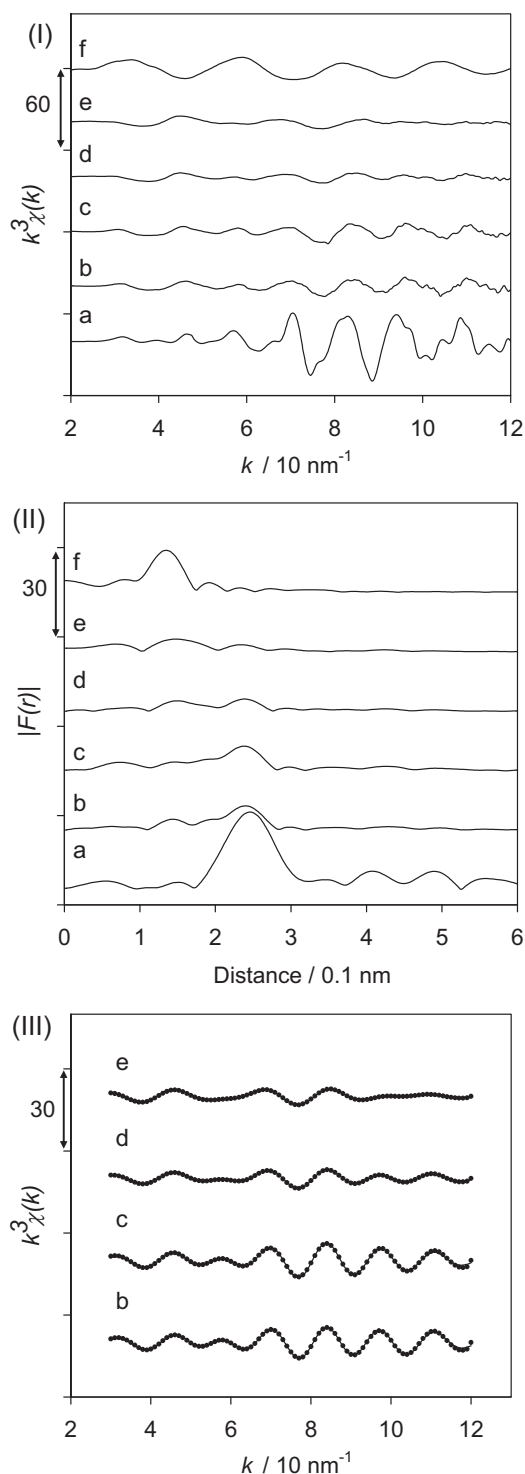


Fig. 2. Results of Mo K-edge EXAFS analysis of various Rh–MoO_x/SiO₂ after the catalytic use. (I) k^3 -weighted EXAFS oscillations. (II) Fourier transform of k^3 -weighted Mo K-edge EXAFS, FT range: 30–120 nm⁻¹. (III) Fourier filtered EXAFS data (solid line) and calculated data (dotted line), Fourier filtering range: 0.129–0.276 nm. (a) Mo foil, (b) Mo/Rh=0.06, (c) Mo/Rh=0.13, (d) Mo/Rh=0.25, (e) Mo/Rh=0.5, and (f) Na₂MoO₄.

because of small difference in the bond distance of Rh–Rh and Rh–Mo, which is given by Mo K-edge EXAFS results (Table 3). In the case of Rh–ReO_x/SiO₂, the presence of the Rh–Re and Rh–Rh bonds is detected. The interaction between ReO_x species and Rh metal surface verified from the side of Rh indicates the presence of the Rh–Re bond. In addition, the CN of the Rh–Re bond increased

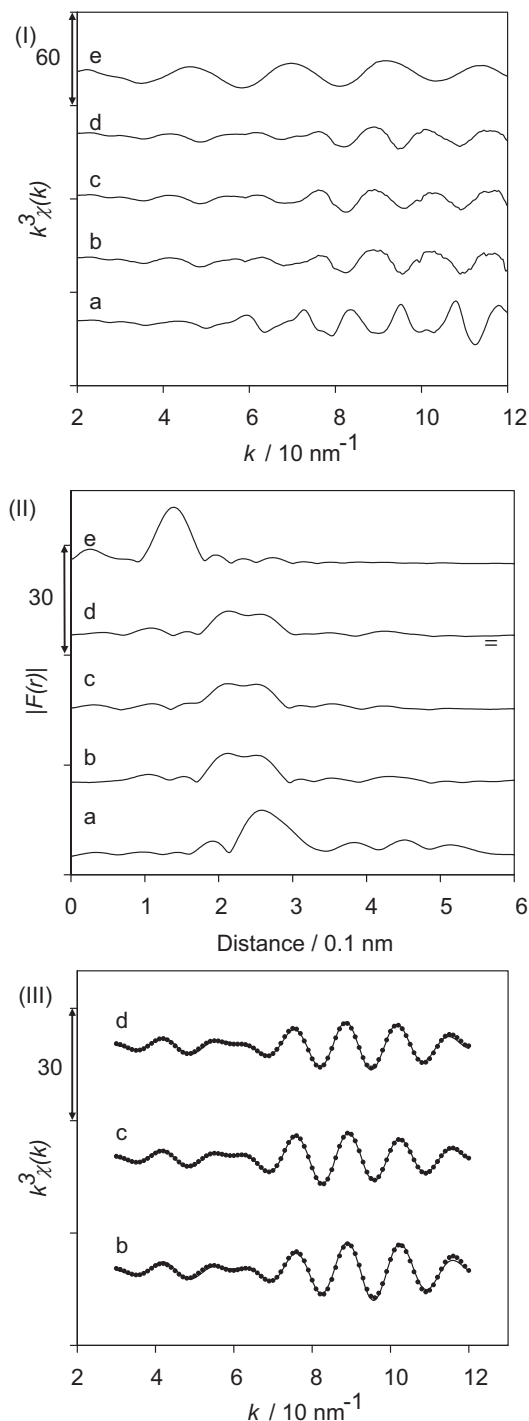


Fig. 3. Results of Re L₃-edge EXAFS analysis of various Rh–ReO_x/SiO₂ after the catalytic use. (I) k^3 -weighted EXAFS oscillations. (II) Fourier transform of k^3 -weighted Re L₃-edge EXAFS, FT range: 30–120 nm⁻¹. (III) Fourier filtered EXAFS data (solid line) and calculated data (dotted line), Fourier filtering range: 0.129–0.301 nm. (a) Re powder, (b) Re/Rh=0.13, (c) Re/Rh=0.25, (d) Re/Rh=0.5, and (e) NH₄ReO₄.

with increasing as the added amount of Re. This tendency indicates the increase of the covering ReO_x species on the surface of Rh metal partially. The CNs of the Rh–Re and Re–Rh bonds meets the relation of Eq. (1) [36].

$$\frac{CN_{Rh-Re}}{CN_{Re-Rh}} = \frac{M_{Re}}{M_{Rh}} \quad (M_{Re}/M_{Rh} : \text{molar ratio of Re to Rh}) \quad (1)$$

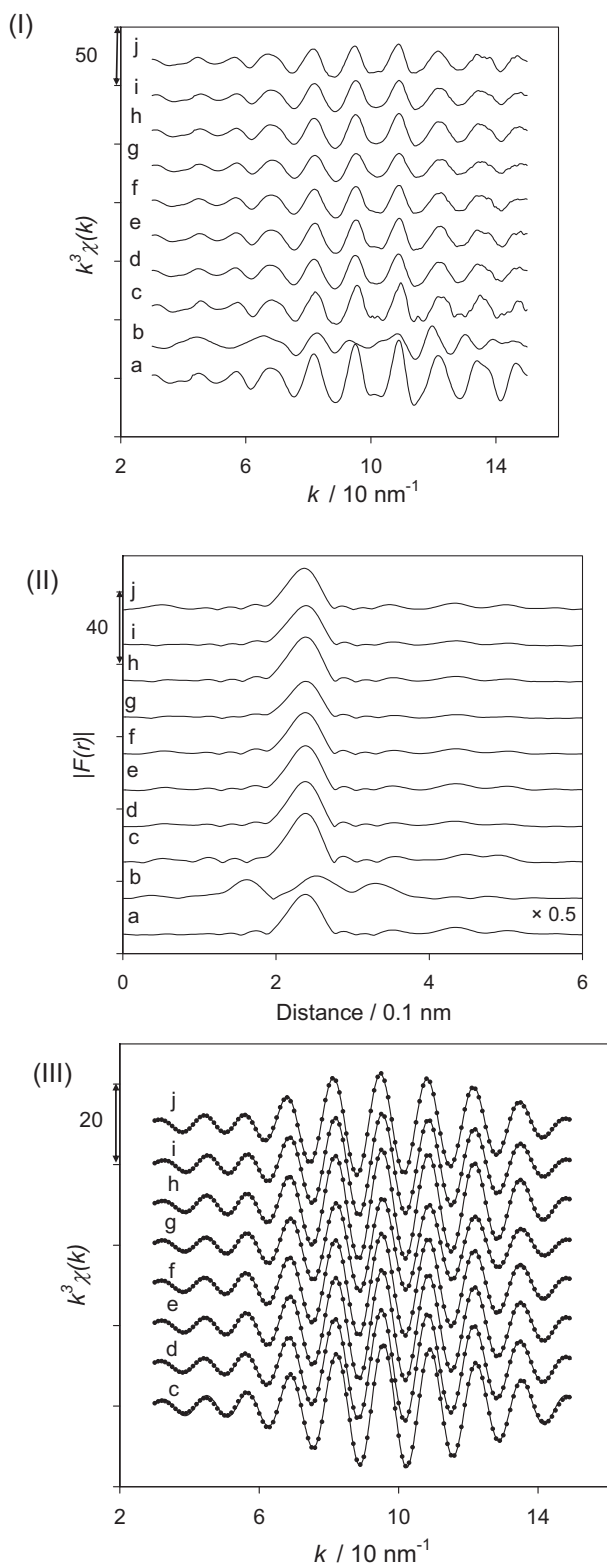


Fig. 4. Results of Rh K-edge EXAFS analysis of various Rh–ReO_x/SiO₂ and Rh–MoO_x/SiO₂ after the catalytic use (Fourier filtering range: 0.166–0.291 nm (Rh/SiO₂, Rh–MoO_x/SiO₂), 0.153–0.288 (Rh–ReO_x/SiO₂)). (I) k^3 -weighted EXAFS oscillations. (II) Fourier transform of k^3 -weighted Rh K-edge EXAFS, FT range: 30–150 nm^{−1}. (III) Fourier filtered EXAFS data (solid line) and calculated data (dotted line). (a) Rh foil, (b) Rh₂O₃, (c) Rh/SiO₂, (d) Mo/Rh=0.06, (e) Mo/Rh=0.13, (f) Mo/Rh=0.25, (g) Mo/Rh=0.5, (h) Re/Rh=0.13, (i) Re/Rh=0.25, and (j) Re/Rh=0.5.

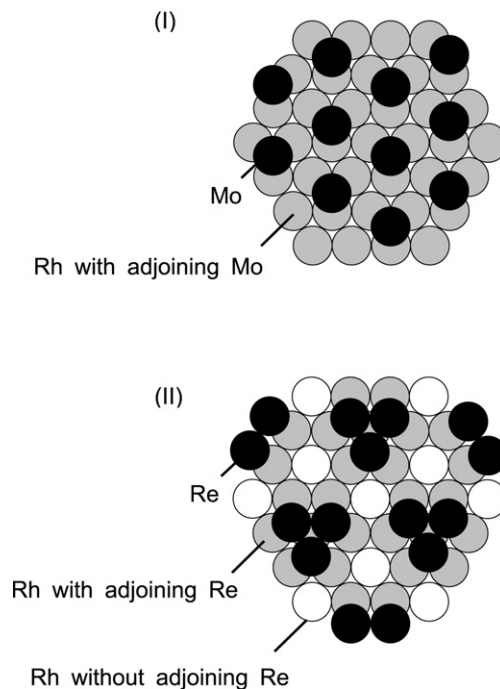


Fig. 5. A model structure of Rh–MoO_x/SiO₂ (Mo/Rh=0.13) (I) and Rh–ReO_x/SiO₂ (Re/Rh=0.13) (II).

On the other hand, the CN of Rh–Rh on Rh–ReO_x/SiO₂ with various Re contents was almost the same that of Rh/SiO₂, which is also suggested by XRD results (Table 2).

Based on the above characterization results and discussion, a model structure of Rh–MoO_x/SiO₂ (Mo/Rh=0.13) and Rh–ReO_x/SiO₂ (Re/Rh=0.13) is described in Fig. 5. In this model, it is assumed that Rh metal surface has (111) structure, which is most stable surface of the fcc metal [37]. Three-fold hollow site is stable adsorption site on the (111) surface. The CN of Mo–Rh (3.0) and Re–Rh (3.8) can be explained by this adsorption site. In the case of Rh–MoO_x/SiO₂ (Mo/Rh=0.13), this interpretation suggests the absence of Mo–Mo bond, and isolated MoO_x species adsorbed on the three-fold hollow site of Rh (111) surface (Fig. 5(I)). The coverage of Mo on Rh (111) surface can be calculated from the dispersion (Rh_s/Rh=0.42, Table 2) and added Mo amount (Mo/Rh=0.13), and it is estimated to be Mo/Rh_s ≅ 1/3. Regarding the coverage of Re on Rh (111) surface, Re/Rh_s is also calculated to be about 1/3 because the dispersion (Rh_s/Rh=0.41, Table 2) and added Re amount (Re/Rh=0.13). At the same time, the CN of the Re–Re bond (CN_{Re–Re}=2, Table 4) suggests the cluster including three Re atoms adsorbed on the three-fold hollow site of Rh (111) surface as described in Fig. 5(II).

In both model structures, the surface Rh atoms with adjoining Mo or Re atom are represented by gray circles and those without adjoining Re are represented by open circles.

3.2. Hydrogenolysis of ethers and polyols over Rh–MoO_x/SiO₂ (Mo/Rh=0.13) and Rh–ReO_x/SiO₂ (Re/Rh=0.13)

The two catalyst, Rh–MoO_x/SiO₂ (Mo/Rh=0.13) and Rh–ReO_x/SiO₂ (Re/Rh=0.13), with the well-defined structures were applied to the hydrogenolysis of various ethers and polyols. The results are listed in Table 6. In the THFA hydrogenolysis, Rh–MoO_x/SiO₂ showed slightly higher activity than Rh–ReO_x/SiO₂ as reported earlier (Entries 1 and 2) [13,18]. The hydrogenolysis of various non-cyclic ethers over Rh–ReO_x/SiO₂ (Re/Rh=0.5) has been reported [17], and the reactivity and selectivity trends are

Table 6
Results of the activity of various ethers and alcohols hydrogenolysis over Rh–Mo_x/SiO₂ (M = Mo or Re, M/Rh = 0.13).^a

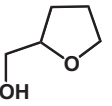
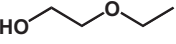
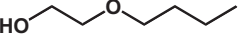
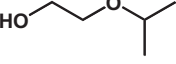
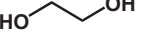
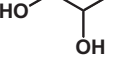
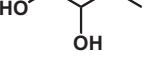
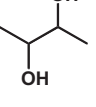

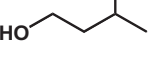
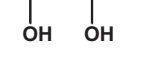



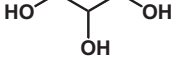
Entry	Reactant	Catalyst	t (h)	Conv. (%)	Selectivity (%)					Reaction rate (mmol g-cat ⁻¹ h ⁻¹)
1	Tetrahydrofurfuryl alcohol 	Rh–MoO _x /SiO ₂	2	7.9	1,5-PeD 99	1,2-PeD 0.0	1-PeOH 0.2	2-MTHF 0.2	Others 0.6	31
2		Rh–ReO _x /SiO ₂	2	6.5	98	0.0	0.8	0.2	1.0	25
3	2-Ethoxyethanol 	Rh–MoO _x /SiO ₂	2	7.5	EtOH 99	Others 1.0				29
4		Rh–ReO _x /SiO ₂	2	8.1	98	2.0				32
5	2-Butoxyethanol 	Rh–MoO _x /SiO ₂	2	6.6	EtOH 33	1-BuOH 64	Others 3.0			26
6		Rh–ReO _x /SiO ₂	2	6.6	32	65	3.0			26
7	2-Isopropoxyethanol 	Rh–MoO _x /SiO ₂	2	9.6	EtOH 39	2-PrOH 60	Others 1.0			38
8		Rh–ReO _x /SiO ₂	2	7.0	39	60	1.0			28
9	Ethylene glycol 	Rh–MoO _x /SiO ₂	2	8.0	EtOH 97	Others 3.0				32
10		Rh–ReO _x /SiO ₂	2	11	97	3.0				43
11	1,2-Propanediol 	Rh–MoO _x /SiO ₂	4	9.3	1-PrOH 80	2-PrOH 20	Others 0.0			18
12		Rh–ReO _x /SiO ₂	4	12	83	17	0.0			23
13	1,2-Butanediol 	Rh–MoO _x /SiO ₂	4	5.1	1-BuOH 80	2-BuOH 17	n-C ₄ H ₁₀ 2.6	Others 0.4		10
14		Rh–ReO _x /SiO ₂	4	7.2	80	15	3.5	1.5		14
15	2,3-Butanediol 	Rh–MoO _x /SiO ₂	4	1.5	2-BuOH 97	n-C ₄ H ₁₀ 3.0	Others 0.0			3
16		Rh–ReO _x /SiO ₂	4	2.5	91	9.0	0.0			5
17	1,3-Propanediol 	Rh–MoO _x /SiO ₂	4	14	1-PrOH 98	Others 2.0				28
18		Rh–ReO _x /SiO ₂	4	7.3	94	6.0				14
19	1,3-Butanediol 	Rh–MoO _x /SiO ₂	4	8.9	1-BuOH 80	2-BuOH 18	n-C ₄ H ₁₀ 1.5	Others 0.5		17
20		Rh–ReO _x /SiO ₂	4	5.5	78	19	2.0	1.0		11
21	2,4-Pentanediol 	Rh–MoO _x /SiO ₂	4	6.5	2-PeOH 98	n-C ₅ H ₁₂ 2.0	Others 0.0			13
22		Rh–ReO _x /SiO ₂	4	3.8	94	6.0	0.0			7
23	3-Methoxy-1-propanol 	Rh–MoO _x /SiO ₂	4	4.6	MeOH 25	1-PrOH 66	Others 9.0			9
24		Rh–ReO _x /SiO ₂	4	3.3	25	66	9.0			6
25	1,4-Butanediol 	Rh–MoO _x /SiO ₂	4	1.0	1-BuOH 95	n-C ₄ H ₁₀ 2.6	Others 2.4			2
26		Rh–ReO _x /SiO ₂	4	0.7	94	2.0	4.0			1

Table 6 (Continued)

Entry	Reactant	Catalyst	t (h)	Conv. (%)	Selectivity (%)					Reaction rate (mmol g-cat ⁻¹ h ⁻¹)
27	1,5-Pentanediol 	Rh–MoO _x /SiO ₂	4	0.5	1-PeOH	Others				1
28		Rh–ReO _x /SiO ₂	4	0.3	93	7.0				1
29	Glycerol 	Rh–MoO _x /SiO ₂	4	7.1	1,3-PrD	1,2-PrD	1-PrOH	2-PrOH	Others	14
30		Rh–ReO _x /SiO ₂	4	9.7	9.6	41	34	14	1.4	19
					21	32	31	15	1.0	19

PeD, pentanediol; PeOH, pentanol; 2-MTHF, 2-methyltetrahydrofuran; MeOH, methanol; EtOH, ethanol; PrOH, propanol; BuOH, butanol; PrD, propanediol.

^a Reaction conditions: 20 wt% aqueous solution (39 mmol substrate + appropriate water), 50 mg catalyst, 393 K reaction temperature, 8.0 MPa initial H₂ pressure.

Table 7

Effect of the concentration of THFA and initial H₂ pressure in the hydrogenolysis of THFA over Rh–MoO_x/SiO₂ (Mo/Rh = 0.13).^a

Concentration of THFA (%)	Initial H ₂ press. (MPa)	Conversion (%)	Selectivity (%)						Reaction rate (mmol g-cat ⁻¹ h ⁻¹)
			1,5-PeD	1,2-PeD	1-PeOH	2-PeOH	2-MTHF	Others	
20	8.0	7.2	99	0.0	0.8	0.0	0.1	0.1	42
30	8.0	8.4	99	0.0	0.8	0.0	0.1	0.1	49
40	8.0	8.7	98	0.0	1.4	0.0	0.4	0.2	50
50	8.0	8.4	98	0.0	1.4	0.0	0.4	0.2	49
60	8.0	7.2	99	0.0	0.8	0.0	0.1	0.1	41
50	6.0	5.6	99	0.0	0.8	0.0	0.1	0.1	33
50	4.0	3.9	98	0.0	1.6	0.0	0.2	0.2	23
50	2.0	1.9	98	0.0	1.7	0.0	0.1	0.1	11

PeD, pentanediol; PeOH, pentanol; 2-MTHF, 2-methyltetrahydrofuran.

^a Reaction conditions: THFA 6 g (58 mmol), water (4–24 g), catalyst 50 mg, reaction temperature 393 K, reaction time 2 h.

almost the same as those of Rh–ReO_x/SiO₂ (Re/Rh = 0.13) shown here. Ethylene glycol mono-ethers such as 2-ethoxyethanol, 2-butoxyethanol, and 2-isopropoxyethanol are non-cyclic ethers with C–O bond neighboring to –CH₂OH group. Regarding these three ethylene glycol ethers, Rh–MoO_x/SiO₂ (Mo/Rh = 0.13) exhibited almost the same activity and selectivity as Rh–ReO_x/SiO₂ (Re/Rh = 0.13) (Entries 3–8). An important point is that the hydrogenolysis of ethylene glycol ethers over Rh–MoO_x/SiO₂ (Mo/Rh = 0.13) and Rh–ReO_x/SiO₂ (Re/Rh = 0.13) gave ethanol as a product derived from ethylene glycol, and this product distribution is explained by the dissociation of the C–O bond neighboring to –CH₂OH group. This behavior can be related to the reaction mechanism as discussed in the next section. As a reference, we also carried out the hydrogenolysis of ethylene glycol (Entries 9 and 10). The reactivity of ethylene glycol was almost the same on both catalysts, and comparable to the reactivity of ethylene glycol mono-ethers. Based on the selective dissociation of the C–O bond neighboring to –CH₂OH group, the catalysts are applicable to the hydrogenolysis of 1,2-diol such as 1,2-propanediol (Entries 11 and 12) and 1,2-butanediol (Entries 13 and 14) including ethylene glycol. On both catalysts, the order of the reactivity was as follows: ethylene glycol > 1,2-propanediol > 1,2-butanediol, and this tendency can be related to the steric hindrance.

Another important point is that the reactivity of 2,3-butanediol (Entries 15 and 16) is much lower than 1,2-butanediol (Entries 13 and 14), indicating that high reactivity is strongly related to the presence of primary OH group, not to the presence of secondary OH group.

Next, we tested the hydrogenolysis of 1,3-diols such as 1,3-propanediol (Entries 17 and 18) and 1,3-butanediol (Entries 19 and 20), and the results are compared to those of 1,2-propanediol (Entries 11 and 12) and 1,2-butanediol (Entries 13 and 14). In the case of Rh–ReO_x/SiO₂ (Re/Rh = 0.13), the order of the reactivity was 1,2-propanediol > 1,3-propanediol and 1,2-butanediol > 1,3-butanediol, and Rh–ReO_x/SiO₂ (Re/Rh = 0.13) is more effective to the hydrogenolysis of the C–O bond

neighboring to –CH₂OH group. In contrast, the order of the reactivity was 1,3-propanediol > 1,2-propanediol and 1,3-butanediol > 1,2-butanediol over Rh–MoO_x/SiO₂ (Mo/Rh = 0.13). The reactivity of 2,4-pentanediol (Entries 21 and 22) and 3-methoxy-1-propanol (Entries 23 and 24) on both catalysts was lower than that of 1,3-propanediol (Entries 17 and 18) and 1,3-butanediol (Entries 19 and 20). It is possible due to both the effect of the length of the carbon chain and the effect of the presence of primary –CH₂OH group. In terms of the hydrogenolysis of the C–O bond dissociation in the –O–C–C–CH₂OH structure, it is concluded that Rh–MoO_x/SiO₂ is more effective than Rh–ReO_x/SiO₂.

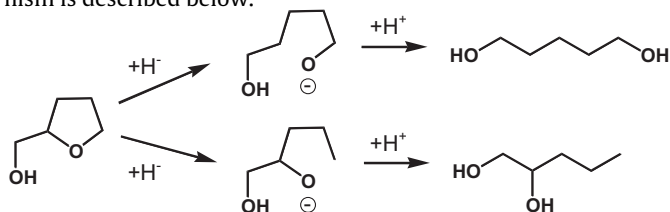
It should be noted that the reactivity of 1,4-butanediol (Entries 25 and 26) and 1,5-pentanediol (Entries 27 and 28) was very low on both catalysts, indicating that both catalysts are not suitable to the hydrogenolysis of the C–O bond in the –O–C–C–C–CH₂OH and –O–C–C–C–C–CH₂OH with longer distance between two C–O bonds.

The hydrogenolysis of glycerol was also tested as a typical triol (Entries 29 and 30). Rh–MoO_x/SiO₂ (Mo/Rh = 0.13) gave lower selectivity to 1,3-propanediol and higher selectivity to 1,2-propanediol than Rh–ReO_x/SiO₂ (Re/Rh = 0.13) in accordance with the reported results under the different conditions [14]. This tendency can be interpreted by higher activity of the C–O bond dissociation in the –O–C–C–CH₂OH structure than that in the –O–C–CH₂OH structure over Rh–MoO_x/SiO₂ (Mo/Rh = 0.13).

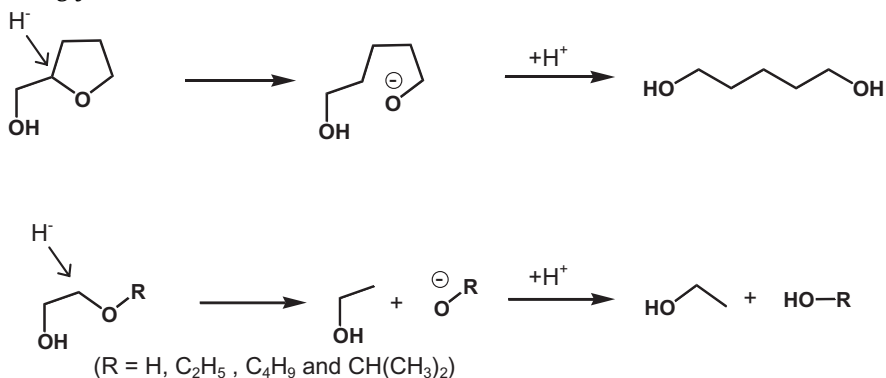
3.3. Reaction mechanism of the hydrogenolysis of ethers and polyols over Rh–MoO_x/SiO₂

The reaction mechanism of the hydrogenolysis of tetrahydrofurfuryl alcohol to 1,5-pentanediol over Rh–ReO_x/SiO₂ has been already proposed [17]. The mechanism via the anion intermediate formed by the attack of hydride and subsequent protonation of the anion (hydride → proton mechanism) has been proposed. The

scheme of the two reaction routes in the hydride→proton mechanism is described below.

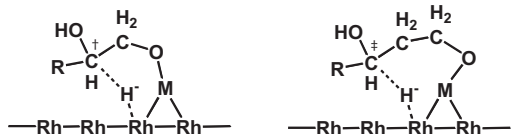


Since the difference in the stability of two anion intermediates is thought to be small, the selective production of 1,5-pentanediol is not determined by the stability of the anion intermediates. One possible explanation is the regioselective hydride attack. The hydride attack to the reactant from the side of $-\text{CH}_2\text{OH}$ group can explain the product distribution in the hydrogenolysis of THFA and ethylene glycol mono-ethers.



Now we discuss the reaction mechanism of Rh–MoO_x/SiO₂. In order to discuss the reaction mechanism, kinetic data are essential. Table 7 lists the result of the effect of the THFA concentration on the catalytic performance of Rh–MoO_x/SiO₂ (Mo/Rh = 0.13). In these experiments, the concentration of THFA was varied by changing the H₂O amount at the constant amount of THFA. Reaction rate was calculated from the converted amount of THFA divided by the reaction time and the catalyst amount. The reaction rate over Rh–MoO_x/SiO₂ was almost constant in this THFA concentration range, suggesting that the strong interaction between THFA and the catalyst surface. Table 7 also shows the effect of H₂ pressure on the THFA hydrogenolysis. The THFA conversion increased linearly with increasing H₂ pressure and the reaction order with respect to H₂ pressure was estimated to be +1. The first reaction order with respect to H₂ pressure indicates that the activation of H₂ is an important step. The kinetic behavior with respect to THFA and H₂ on Rh–MoO_x/SiO₂ was just the same as that on Rh–ReO_x/SiO₂ [17], suggesting the formation of the reactive hydride on Rh–MoO_x/SiO₂ like Rh–ReO_x/SiO₂.

Another important point is the regioselectivity of the hydride attack, which can be estimated from the results of the activity tests of 1,2-diols and 1,3-diols as shown below.



Hydrogenolysis of 1,2-diol Hydrogenolysis of 1,3-diol

Higher reactivity of 1,2-diols than that of 1,3-diols on Rh–ReO_x/SiO₂ suggests that the hydride attack to C[†] in $-\text{O}-\text{C}^\dagger-\text{CH}_2\text{OH}$ structure is more preferable to that is $-\text{O}-\text{C}^\ddagger-\text{CH}_2\text{OH}$. In contrast, higher reactivity of 1,3-diols than that of 1,2-diols on Rh–MoO_x/SiO₂ suggests that the hydride attack to C[†] in $-\text{O}-\text{C}^\dagger-\text{CH}_2\text{OH}$ is more preferable. At present, the reason for the different regioselectivity of the hydride attack

between Mo and Re modifier is not elucidated sufficiently and further investigation is necessary, although the difference can be caused by the different structure of two-dimensional ReO_x clusters and isolated MoO_x species.

4. Conclusions

1. On Rh–MoO_x/SiO₂ (Mo/Rh = 0.13–0.5) and Rh–ReO_x/SiO₂ (Re/Rh = 0.13–0.5), Rh metal particles and low valent Mo and Re cation species with higher dispersion are formed during the H₂ reduction.
2. The average size of Rh metal particles was not influenced by the added amount of Mo and Re in the range of Mo/Rh ≤ 0.5 and Re/Rh ≤ 0.5.
3. On Rh–MoO_x/SiO₂ (Mo/Rh = 0.13) and Rh–ReO_x/SiO₂ (Re/Rh = 0.13), almost all the added Mo and Re species interacts

with Rh metal surface. The EXAFS analysis show the interaction of the Mo and Re species with Rh metal surface is direct, and they also show that the formation of the isolated MoO_x species and the small ReO_x cluster on the Rh metal surface.

4. The reactivity in the hydrogenolysis of tetrahydrofurfuryl alcohol, various diols and the ethers of the diols over Rh–MoO_x/SiO₂ and Rh–ReO_x/SiO₂ were compared, and it is verified that high reactivity is related to the presence of primary $-\text{CH}_2\text{OH}$ group on the substrates.
5. In the case of Rh–MoO_x/SiO₂, the reactivity in the hydrogenolysis of the C–O bond of $-\text{O}-\text{C}-\text{CH}_2\text{OH}$ was higher than that of $-\text{O}-\text{C}^\ddagger-\text{CH}_2\text{OH}$. In contrast, in the case of Rh–ReO_x/SiO₂, the reactivity in the C–O bond of $-\text{O}-\text{C}^\ddagger-\text{CH}_2\text{OH}$ was higher than that of $-\text{O}-\text{C}-\text{CH}_2\text{OH}$. The different reactivity is thought to be due to the difference in the local structure of Mo and Re.

Acknowledgement

This work was supported by Grant-in-Aid for JSPS Fellows, and a part of this research is funded by the Cabinet Office, Government of Japan through its “Funding Program for Next Generation World-Leading Researchers”.

Appendix A. Supplementary data

Supplementary data associated with this article can be found, in the online version, at doi:10.1016/j.apcatb.2011.09.015.

References

- [1] G.L. Haller, D.E. Resasco, Adv. Catal., vol. 36, Academic Press, New York, 1989, pp. 173–235.
- [2] S.J. Tauster, Acc. Chem. Res. 20 (1987) 389–394.
- [3] B.J. Kip, E.G.F. Hermans, J.H.M.C. Van Wolput, N.M.A. Hermans, J. Van Grondelle, R. Prins, Appl. Catal. 35 (1987) 109–139.

- [4] K. Tomishige, I. Furikado, T. Ymagishi, S. Ito, K. Kunimori, *Catal. Lett.* 103 (2005) 15–21.
- [5] S. Ishiguro, S. Ito, K. Kunimori, *Catal. Today* 45 (1998) 197–201.
- [6] S. Ito, C. Chibana, K. Nagashima, S. Kameoka, K. Tomishige, K. Kunimori, *Appl. Catal. A: Gen.* 236 (2002) 113–120.
- [7] T. Yamagishi, I. Furikado, S. Ito, T. Miyao, S. Naito, K. Tomishige, K. Kunimori, *J. Mol. Catal. A* 244 (2006) 201–212.
- [8] T. Yamagishi, S. Ito, K. Tomishige, K. Kunimori, *Catal. Commun.* 6 (2005) 421–425.
- [9] S. Ito, T. Fujimori, K. Nakagawa, K. Yuzaki, K. Kunimori, *Catal. Today* 57 (2000) 247–254.
- [10] T. Uchijima, *Catal. Today* 28 (1996) 105–117.
- [11] M. Schlaf, *Dalton Trans.* (2006) 4645–4653.
- [12] A. Corma, S. Iborra, A. Velty, *Chem. Rev.* 107 (2007) 2411–2502.
- [13] S. Koso, I. Furikado, A. Shimao, T. Miyazawa, K. Kunimori, K. Tomishige, *Chem. Commun.* (2009) 2035–2037.
- [14] Y. Shinmi, S. Koso, T. Kubota, Y. Nakagawa, K. Tomishige, *Appl. Catal. B: Environ.* 94 (2010) 318–326.
- [15] Y. Nakagawa, K. Tomishige, *Catal. Surv. Asia* 15 (2011) 111–116.
- [16] Y. Nakagawa, K. Tomishige, *Catal. Sci. Technol.* 1 (2011) 179–190.
- [17] S. Koso, Y. Nakagawa, K. Tomishige, *J. Catal.* 280 (2011) 221–229.
- [18] S. Koso, N. Ueda, Y. Shinmi, K. Okumura, T. Kizuka, K. Tomishige, *J. Catal.* 267 (2009) 89–92.
- [19] S.R. Sashital, J.B. Cohen, R.L. Burwell Jr., J.B. Butt, *J. Catal.* 50 (1977) 479–493.
- [20] J.W. Cook, D.E. Sayers, *J. Appl. Phys.* 52 (1981) 5024–5031.
- [21] K. Okumura, J. Amano, N. Yasunobu, M. Niwa, *J. Phys. Chem. B* 104 (2000) 1050–1057.
- [22] K. Okumura, S. Matsumoto, N. Nishiaki, M. Niwa, *Appl. Catal. B: Environ.* 40 (2003) 151–159.
- [23] A.L. Ankudinov, B. Ravel, J.J. Rehr, S.D. Conradson, *Phys. Rev. B* 58 (1998) 7565–7576.
- [24] K. Tomishige, K. Asakura, Y. Iwasawa, *J. Catal.* 149 (1994) 70–80.
- [25] Y. Amada, S. Koso, Y. Nakagawa, K. Tomishige, *ChemSusChem* 3 (2010) 728–736.
- [26] Y. Nakagawa, Y. Shinmi, S. Koso, K. Tomishige, *J. Catal.* 272 (2010) 191–194.
- [27] Y. Amada, Y. Shinmi, S. Koso, T. Kubota, Y. Nakagawa, K. Tomishige, *Appl. Catal. B: Environ.* 105 (2011) 117–127.
- [28] P. Reyes, C. Rodríguez, G. Pecchi, J.L.G. Fierro, *Catal. Lett.* 69 (2000) 27–32.
- [29] A.J. Marchi, E.J. Lede, F.G. Requejo, M. Rentería, S. Irusta, E.A. Lombardo, E.E. Miró, *Catal. Lett.* 48 (1997) 47–54.
- [30] K. Tomishige, A. Okabe, K. Fujimoto, *Appl. Catal. A: Gen.* 194 (2000) 383–393.
- [31] R. Ueda, T. Kusakari, K. Tomishige, K. Fujimoto, *J. Catal.* 194 (2000) 14–22.
- [32] K. Chen, S. Koso, T. Kubota, Y. Nakagawa, K. Tomishige, *ChemCatChem* 2 (2010) 547–555.
- [33] Y. Izumi, K. Konishi, M. Tsukahara, D.M. Obaid, K. Aika, *J. Phys. Chem. C* 111 (2007) 10073–10081.
- [34] D.D. Beck, T.W. Capehart, C. Wong, D.N. Belton, *J. Catal.* 144 (1993) 311–324.
- [35] T. Miyazawa, K. Okumura, K. Kunimori, K. Tomishige, *J. Phys. Chem. C* 112 (2008) 2574–2583.
- [36] H. Tanaka, R. Kaino, K. Okumura, T. Kizuka, Y. Nakagawa, K. Tomishige, *Appl. Catal. A: Gen.* 378 (2010) 175–186.
- [37] M.C. Aguirre, J.G. Fierro, P. Reyes, *React. Kinet. Catal. Lett.* 84 (2005) 351–358.
- [38] K. Kunimori, T. Uchijima, M. Yamada, H. Matsumoto, T. Hattori, Y. Murakami, *Appl. Catal.* 4 (1982) 67–81.